CHEMISTRY OF MATERIALS

Article

pubs.acs.org/cm

Trimethylaluminum as the Metal Precursor for the Atomic Layer Etching of Al_2O_3 Using Sequential, Self-Limiting Thermal Reactions

Younghee Lee,[†] Jaime W. DuMont,[†] and Steven M. George*[,†,‡]

[†]Department of Chemistry and Biochemistry, [‡]Department of Mechanical Engineering, University of Colorado, Boulder, Colorado 80309, United States

Supporting Information

ABSTRACT: Trimethylaluminum (TMA, $Al(CH_3)_3$) was used as the metal precursor, together with HF, for the atomic layer etching (ALE) of Al_2O_3 using sequential, self-limiting thermal reactions. Al_2O_3 ALE using TMA demonstrates that other metal precursors, in addition to $Sn(acac)_2$, can be employed for Al_2O_3 ALE. The use of TMA for Al_2O_3 ALE is especially interesting because TMA can also be used for Al_2O_3 atomic layer deposition (ALD). Quartz crystal microbalance (QCM) experiments monitored Al_2O_3 ALE at temperatures from 250 to 325 °C. The Al_2O_3 ALE was linear versus the number of HF and TMA reaction cycles. The QCM studies showed that the sequential HF and TMA reactions were self-limiting versus reactant exposure. The Al_2O_3 etching rates increased at higher temperatures. The QCM analysis measured mass change per cycle (MCPC) values that varied from −4.2 ng/(cm^2 cycle) at 250 °C to −23.3 ng/(cm^2 cycle) at 325 °C. These MCPCs correspond to Al_2O_3 etch rates from 0.14 Å/cycle at 250 °C to 0.75 Å/cycle at 325 °C. X-ray reflectivity and spectroscopic ellipsometry analyses confirmed the linear removal of Al_2O_3 and etching rates. Fourier transform infrared spectroscopy measurements monitored Al_2O_3 ALE by observing the loss of infrared absorbance from Al−O stretching vibrations. Surface intermediates were also identified after the HF and TMA exposures. Al_2O_3 ALE with TMA is believed to occur by the reaction $Al_2O_3 + 4Al(CH_3)_3 + 6HF \rightarrow 6AlF(CH_3)_2 + 3H_2O$. The proposed mechanism involves fluorination and ligand-exchange reactions. The HF exposure fluorinates the Al_2O_3 and forms an AlF_3 surface layer and H_2O as a volatile reaction product. During the ligand-exchange transmetalation reaction, TMA accepts F from the AlF_3 surface layer and donates CH_3 to produce volatile $AlF(CH_3)_2$ reaction products. The QCM measurements were consistent with an AlF_3 surface layer thickness of 3.0 Å on Al_2O_3 after the HF exposures. The larger etch rates at higher temperatures were attributed to the removal of a larger fraction of the AlF_3 surface layer by TMA exposures at higher temperatures.

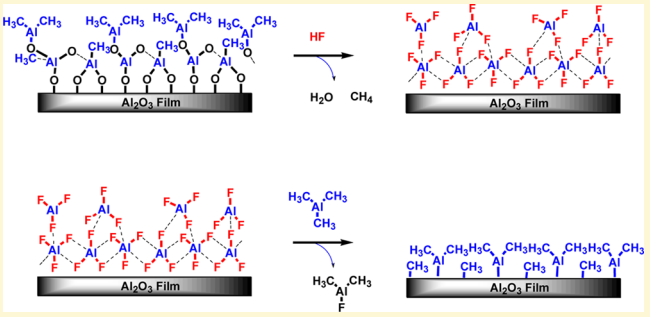

I. INTRODUCTION

Atomic layer etching (ALE) involves the removal of thin films based on sequential, self-limiting surface reactions.[1,2] ALE is the reverse of atomic layer deposition (ALD).[3,4] Atomic layer processes, such as ALE and ALD, are crucial to engineer film thicknesses with atomic scale precision and to build nanoscale semiconductor devices.[1,2] Most of the reported ALE processes to date have used halogenation reactions followed by energetic ion or noble gas atom bombardment to etch the material.[1,5,6] The use of energetic ions or atoms for etching is useful to achieve anisotropic etching.[1,2] In contrast, thermal ALE processes enable conformal and isotropic etching of three-dimensional structures.[2] Thermal ALE may also achieve etching without damaging the underlying film.

Thermal ALE processes have been developed only recently. The first reported thermal ALE system was Al_2O_3 ALE using HF and $Sn(acac)_2$ as the reactants.[7,8] Subsequently, HfO_2 ALE[9] and AlF_3 ALE[10] were also demonstrated using HF and $Sn(acac)_2$. The chemistry of thermal ALE is based on fluorination and ligand-exchange reactions. $Sn(acac)_2$ is a good metal precursor for the ligand-exchange reaction. The ligand-exchange reaction can be characterized as a metal exchange transmetalation[11] or a redistribution[12] reaction. In the ligand-exchange reaction, ligands are transferred between adjacent metal centers.[13] The transition state is generally believed to be a four-center ring based on a variety of transmetalation reaction studies, such as Stille cross-coupling between Pd and organotin compounds.[13] For thermal ALE, the four-center ring would be formed by the metal in the metal precursor and the metal in the metal fluoride with fluorine and ligand bridging species. Fluorine facilitates the four-center ring transition state because of its ability to form bimetallic bridges.[14]

Transmetalation reactions are known to be favored if an empty orbital is available on both metals.[13] In addition, thermodynamics predicts that the halide atom prefers to

Received: January 10, 2016
Revised: April 10, 2016
Published: April 11, 2016

DOI: 10.1021/acs.chemmater.6b00111
Chem. Mater. 2016, 28, 2994−3003

transfer to the most electropositive atom during transmetalation.[13] Sn(II) compounds with SnX_2 stoichiometry like $Sn(acac)_2$ are good candidates for transmetalation.[15,16] Sn has a medium electronegativity of 1.8. Sn(II) complexes with SnX_2 stoichiometry also have an empty 5p orbital and an unshared 5s electron pair.[17,18] The empty 5p orbital and unshared 5s electron pair yield Lewis acid and Lewis base properties that give chemical versatility to $Sn(acac)_2$. Sn also can form relatively strong bonds with fluorine.[18]

Other metal precursors may also display favorable properties for the ligand-exchange reaction. Another promising metal precursor is trimethylaluminum (TMA). TMA has an open outer shell and is a strong Lewis acid because Al has only three valence electrons and does not obey the octet rule. Al has a low electronegativity of 1.5. Al is also known to form strong bonds with fluorine.[19] TMA is a popular reactant resulting from its high volatility and excellent reactivity. For example, sequential TMA and H_2O exposures are well-known to form Al_2O_3 ALD films.[20] The use of TMA for Al_2O_3 ALE is particularly intriguing because TMA could serve to either grow Al_2O_3 by ALD or etch Al_2O_3 by ALE depending on the other reactant used together with TMA.

The use of different metal precursors for thermal ALE could also lead to selective ALE. Different metal precursors introduce various ligands that may transfer during the ligand-exchange transmetalation reaction. If the transferred ligand produces a metal product that is stable and volatile, then the metal product may leave the surface and produce etching. If the possible metal product is not stable or volatile, then the ligand-exchange reaction may not occur or may not produce a volatile etch product. In the previous work using $Sn(acac)_2$ as the metal precursor for ligand-exchange, $Sn(acac)_2$ transferred acac ligands to produce stable and volatile Al and Hf reaction products.[7−10] In comparison, TMA can transfer CH_3 ligands that may lead to reaction products with different stabilities and volatilities that may provide for selective ALE.

In this paper, sequential exposures of HF and TMA were employed for thermal Al_2O_3 ALE. The etching rates and individual HF and TMA reactions during thermal Al_2O_3 ALE were examined using quartz crystal microbalance (QCM) studies. The Al_2O_3 film thicknesses versus number of sequential HF and TMA exposures were also measured using X-ray reflectivity (XRR) and spectroscopic ellipsometry analyses. In addition, Fourier transform infrared (FTIR) spectroscopy measurements were used to observe the loss of infrared absorbance from Al−O stretching vibrations and monitor the surface species during the sequential HF and TMA exposures. These studies demonstrate that other metal precursors, in addition to $Sn(acac)_2$, can be employed for the ligand-exchange reactions in thermal ALE.

II. EXPERIMENTAL SECTION

II.A. *In situ* QCM Studies in Viscous Flow Reactor. The ALE reactions were performed in a viscous flow, hot wall ALD reactor.[21] An *in situ* quartz crystal microbalance (QCM) was mounted inside of the isothermal, hot wall ALD reactor. The quartz crystal (gold coated and polished, RC-cut 6 MHz, Colnatec) was placed in a sensor housing (BSH-150, Inficon). This sensor housing was then sealed with high temperature epoxy (Epo-Tek H21D, Epoxy technology). The mass changes during the ALE reactions were recorded by a thin film deposition monitor (Maxtek TM-400, Inficon). A proportional-integral-derivative (PID) temperature controller (2604, Eurotherm) maintained the reaction temperature at 250, 275, 300, and 325 °C. The temperature was controlled to within ±0.04 °C of the exact set point. This temperature stability was important for accurate QCM measurements. The change of the reaction temperature required more than 2 h of stabilization. A capacitance manometer (Baratron 121A, MKS) monitored the pressure in the reactor.

The Al_2O_3 films were grown on the QCM crystal with Al_2O_3 ALD using TMA (97%, Sigma-Aldrich) and H_2O (Chromasolv for HPLC, Sigma-Aldrich). The Al_2O_3 ALE reactions were accomplished using sequential exposures of TMA and HF derived from HF-pyridine (70 wt % HF, Sigma-Aldrich). HF-pyridine is a liquid and HF gas has a vapor pressure of 90−100 Torr over the HF-pyridine solution at room temperature.[9] The pyridine partial pressure is negligible.[22] The use of gaseous HF from the HF-pyridine solution allows for the safe handling of anhydrous HF. HF-pyridine was transferred to a gold-plated stainless steel bubbler using a dry N_2-filled glovebag. The HF-pyridine, TMA, and H_2O precursors were at room temperature.

A constant flow of 150 sccm of ultra high purity (UHP) N_2 gas was delivered into the reactor using mass flow controllers (Type 1179A, MKS). An additional flow of 20 sccm of N_2 gas through a metering bellows-sealed valve (SS-4BMG, Swagelok) prevented deposition on the backside of the QCM crystal.[21] The total N_2 gas flow of 170 sccm produced a base pressure of ∼1 Torr in the reactor pumped by a mechanical pump (Pascal 2015SD, Alcatel).

II.B. Si Wafers, X-ray Reflectivity, Spectroscopic Ellipsometry and X-ray Photoelectron Spectroscopy. Al_2O_3 ALD films were grown on boron-doped Si(100) wafers (p-type, Silicon Valley Microelectronics). These Al_2O_3 ALD films were used as the substrates for the ALE reactions. The bare Si substrates were cut into samples with dimensions of 2.5 cm by 2.5 cm before the Al_2O_3 ALD.

The *ex situ* X-ray reflectivity (XRR) scans were measured by a high resolution X-ray diffractometer (Bede D1, Jordan Valley Semiconductors) using Cu Kα (λ = 1.540 Å) radiation. The filament voltage and current in the X-ray tube were 40 kV and 35 mA, respectively. A 10 arcsec step size and a 5 s acquisition time were used for recording all XRR scans with a range of 300 to 6000 arcsec. The analysis software (Bede REFS, Jordan Valley Semiconductors) determined film thickness, film density and surface roughness by fitting the XRR scans.

Ellipsometry was performed using a spectroscopic ellipsometer (M-2000, J. A. Woollam) with a spectral range of 240 to 1700 nm and an incidence angle of 75°. The analysis software (CompleteEASE, J. A. Woollam) fitted the Ψ and Δ values based on a Sellmeier model to determine the thicknesses and refractive index of the film.[23] The film composition was confirmed using X-ray photoelectron spectroscopy (XPS). The XPS instrument (PHI 5600) was equipped with a monochromatic Al Kα X-ray source.

II.C. *In situ* Fourier Transform Infrared (FTIR) Spectroscopy Studies. The *in situ* FTIR spectroscopy studies were performed in a reactor equipped with an FTIR spectrometer.[24] The FTIR experiments utilized high surface area, ZrO_2 nanoparticles (99.95%, US Research Nanomaterials) with an average diameter of 20 nm. The ZrO_2 nanoparticles absorb infrared radiation between ∼400−800 cm^{-1} and leave an open window at >800 cm^{-1} to monitor absorbance from the surface species.

The ZrO_2 nanoparticles were mechanically pressed into a tungsten grid support to obtain the transmission FTIR measurements.[25,26] The tungsten grids were 2 cm × 3 cm, 50 μm thick, with 100 grid lines per inch. The tungsten grid could be resistively heated and temperature controlled as described previously.[24,26] The Al_2O_3 films were grown on the ZrO_2 nanoparticles with Al_2O_3 ALD using TMA (97%, Sigma-Aldrich) and H_2O (Chromasolv for HPLC, Sigma-Aldrich). The Al_2O_3 ALE reactions were performed using sequential exposures of TMA (97%, Sigma-Aldrich) and HF derived from HF-pyridine (70 wt % HF, Sigma-Aldrich).

Static dosing of both the ALD and ALE precursors was performed to achieve self-limiting behavior on the high surface area particle substrates. Each reactant exposure consisted of a ∼ 1 Torr static dose for 10 s followed by a 240 s purge. The Al_2O_3 film on the ZrO_2 nanoparticles was grown using 15 cycles of Al_2O_3 ALD at 150 °C. Subsequently, 8 cycles of Al_2O_3 ALE were performed at 300 °C.

DOI: 10.1021/acs.chemmater.6b00111
Chem. Mater. 2016, 28, 2994−3003

III. RESULTS AND DISCUSSION

III.A. QCM Measurements. Figure 1 shows the mass change during 100 ALE cycles using sequential exposures of

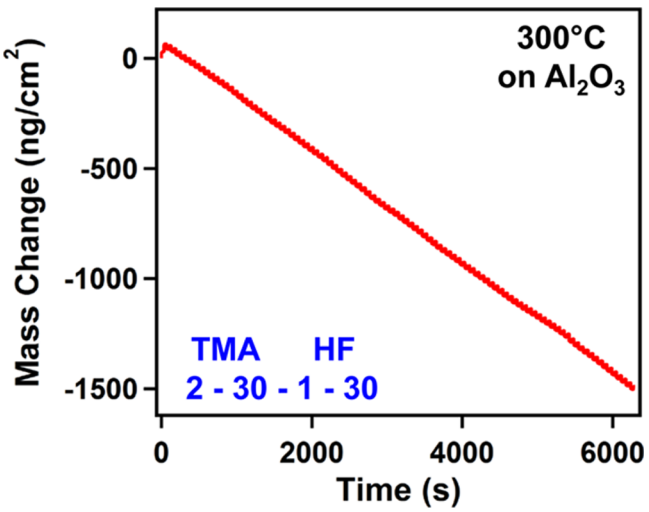

Figure 1. Mass change versus time for Al_2O_3 ALE using sequential TMA and HF exposures at 300 °C.

TMA and HF on an Al_2O_3 substrate at 300 °C. The initial Al_2O_3 ALD film on the QCM crystal was deposited by 100 cycles of Al_2O_3 ALD using TMA and H_2O at 300 °C. One ALE cycle consisted of a TMA dose of 2.0 s, an N_2 purge of 30 s, a HF dose of 1.0 s, and a second N_2 purge of 30 s. This reaction sequence is represented as 2−30−1−30. Pressure transients during TMA and HF exposures were ∼40 mTorr and ∼80 mTorr, respectively. These pressure transients were observed on top of the base pressure of ∼1 Torr in the reactor.

Figure 1 displays linear etching of the Al_2O_3 film. A slope of the mass change versus time yields a mass change per cycle (MCPC) of −15.9 ng/(cm^2 cycle). This MCPC represents the removal of 9.4×10^{13} "Al_2O_3" units/(cm^2 cycle). This MCPC is also equivalent to an etch rate of 0.51 Å/cycle based on the Al_2O_3 ALD film density of 3.1 g/cm^3 determined by XRR. All ALE cycles show mass loss except during the first ALE cycle. The first cycle displays mass gains of ΔM_{TMA} = 32 ng/cm^2 and ΔM_{HF} = 33 ng/cm^2.

The mass gain for ΔM_{TMA} during the first TMA exposure is attributed to the formation of $AlCH_3$* surface species on the initial hydroxylated Al_2O_3 substrate. The asterisks designate a surface species. The mass gain for ΔM_{HF} during the first HF exposure is attributed to the fluorination of the Al_2O_3 substrate. The HF exposure reacts with $AlCH_3$* to form AlF* surface species. HF exposure can also fluorinate the underlying Al_2O_3 film to form an AlF_3 surface layer. The reaction $Al_2O_3 + 6HF \rightarrow 2AlF_3 + 3H_2O$ is spontaneous with ΔG= −49 kcal at 300 °C.[27] This first cycle establishes the initial AlF_3 layer on the Al_2O_3 substrate.

Figure 2 shows an enlargement of the mass changes versus time at 300 °C in the steady state region of Figure 1. Each reactant exposure leads to pronounced mass changes. The TMA exposure results in a mass decrease. This behavior indicates TMA can remove the AlF_3 surface layer on the Al_2O_3 film. A mass loss of ΔM_{TMA} = −29 ng/cm^2 was observed after 2.0 s of TMA exposure. In contrast, the HF exposure leads to mass gain. A mass gain of ΔM_{HF} = 13 ng/cm^2 was observed after 1.0 s of HF exposure. This mass gain is consistent with the

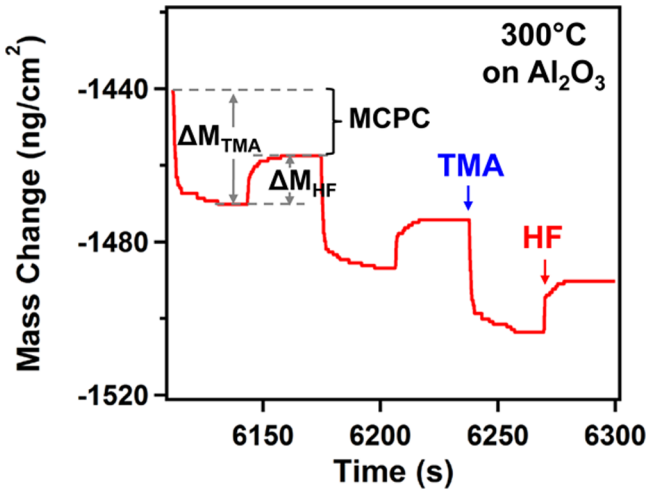

Figure 2. Enlargement of linear region of Figure 1 showing the individual mass changes during the sequential TMA and HF exposures at 300 °C.

fluorination of Al_2O_3 to form an AlF_3 surface layer. This AlF_3 surface layer is then ready for the ligand-exchange reaction during the next TMA exposure.

Figure 3 shows the MCPC and the ΔM_{TMA}/MCPC ratio during 100 Al_2O_3 ALE cycles at 300 °C. The ΔM_{TMA} and

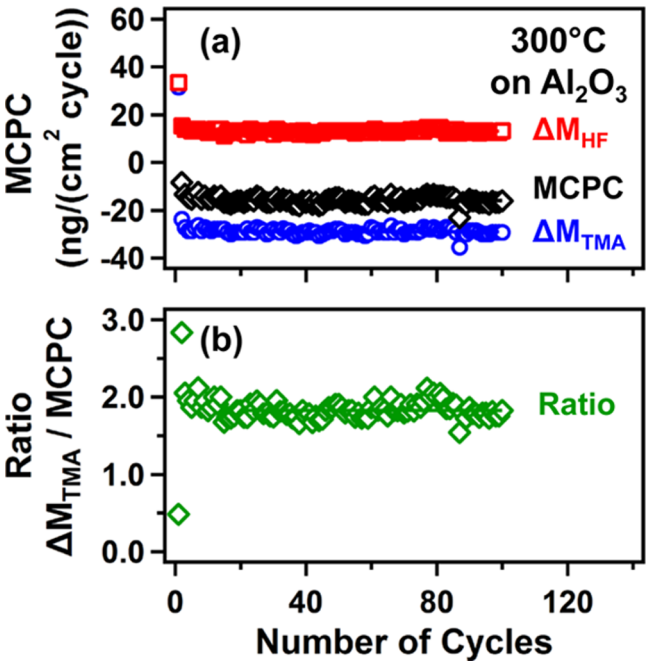

Figure 3. (a) Mass change after the TMA exposure (ΔM_{TMA}), mass change after the HF exposure (ΔM_{HF}) and mass change per cycle (MCPC) versus number of ALE cycles at 300 °C. (b) ΔM_{TMA}/MCPC ratio versus number of ALE cycles.

ΔM_{HF} mass changes are very constant. The MCPC is defined by MCPC = $\Delta M_{TMA} + \Delta M_{HF}$. Figure 3a displays ΔM_{TMA}, ΔM_{HF} and MCPC for the same 100 cycles of Al_2O_3 ALE reaction at 300 °C shown in Figure 1. A short nucleation period was observed before reaching steady state with MCPC = −15.9 ng/(cm^2 cycle). Figure 3b displays the ΔM_{TMA}/MCPC ratio during the same 100 cycles. The ΔM_{TMA}/MCPC ratio shows a steady-state value of 1.8 after the first three ALE cycles. The

DOI: 10.1021/acs.chemmater.6b00111
Chem. Mater. 2016, 28, 2994−3003

ΔM_{TMA}/MCPC ratio will be employed to define the stoichiometry of the Al_2O_3 ALE reactions.

The self-limiting behavior can be confirmed by monitoring mass change as a function of exposure for each reactant. Self-limiting ALE reactions are important for conformal or isotropic etching. Figure 4 examines the self-limiting nature of the Al_2O_3

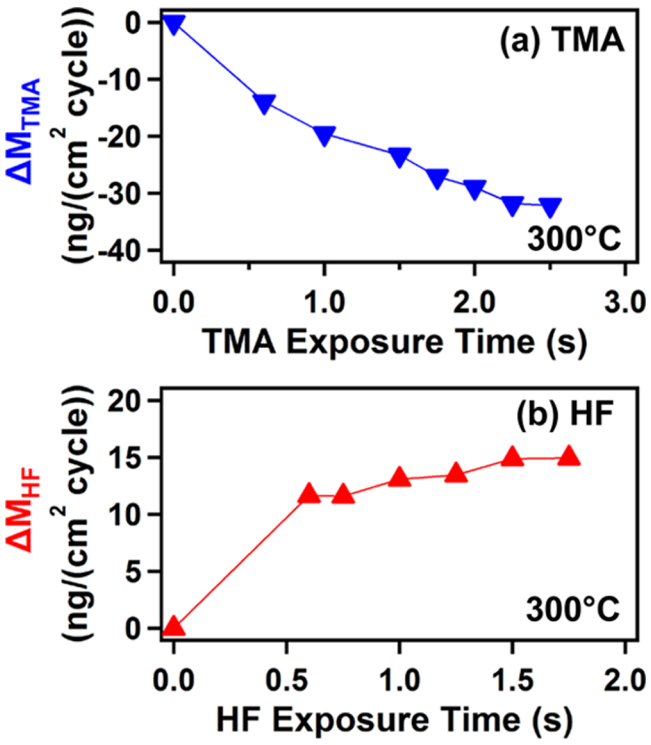

Figure 4. (a) Mass change after TMA exposure (ΔM_{TMA}) versus TMA exposure time at 300 °C (b) Mass change after HF exposure (ΔM_{HF}) versus HF exposure time at 300 °C.

ALE reactions at 300 °C. Figure 4a shows ΔM_{TMA}, the mass change after the TMA exposure, using different TMA exposure times with a single 1.0 s exposure of HF. A constant N_2 purge of 30 s was used after each exposure. This reaction sequence can be represented as x−30−1−30. ΔM_{TMA} versus the TMA exposure time decreases and levels off slowly.

Nearly self-limiting behavior at ΔM_{TMA} = −29 ng/cm^2 is observed after 2.0 s of TMA exposure. This slow approach to self-limiting behavior may result from the difficulty in removing all of the AlF_3 surface layer. An initial fraction of the AlF_3 surface layer may be easily removed by TMA. The removal of more of the AlF_3 surface layer may then become progressively difficult. Additional analysis of the temperature dependence of the TMA reaction presented below will reveal that only a fraction of the AlF_3 surface layer is removed even at the highest temperatures.

Figure 4b monitors ΔM_{HF}, the mass change after the HF exposure, using different HF exposure times with a single 2.0 s exposure of TMA. This reaction sequence can be denoted as 2−30−x−30. ΔM_{HF} versus the HF exposure time increases and then levels off at approximately ΔM_{HF} = 13 ng/(cm^2 cycle) after a 1.0 s HF exposure. This self-limiting behavior is consistent with HF fluorinating the Al_2O_3 film and forming an AlF_3 surface layer that passivates the underlying Al_2O_3 film.

This surface fluoride layer on Al_2O_3 is similar to the native oxide layers formed on metals[28−30] or silicon[31−33] that protect the metals or silicon from further oxidation. The AlF_3 surface layer is expected to passivate the Al_2O_3 film because the Pilling-Bedworth ratio, R_{PB}, is >1.[34] R_{PB} is the ratio of the molar volume, V, of the top layer to the molar volume of the underlying material. The molar volume, V = M/ρ, where M is the molar mass and ρ is the density. $V_{AlF3} = M_{AlF3}/\rho_{AlF3}$= 29 cm^3/mol because M_{AlF3} = 84 g/mol and ρ_{AlF3} = 2.9 g/cm^3. $V_{Al2O3} = M_{Al2O3}/\rho_{Al2O3}$ = 33 cm^3/mol because M_{Al2O3} = 102 g/mol and ρ_{Al2O3}= 3.1 g/cm^3. Using these values, $R_{PB} = (V_{AlF3} \times 2)/V_{Al2O3}$ = 1.8. The factor of 2 accounts for the aluminum stoichiometry difference between AlF_3 and Al_2O_3.

Figure 5 displays the mass change during 100 ALE cycles at 250, 275, 300, and 325 °C using the reaction sequence of 2−

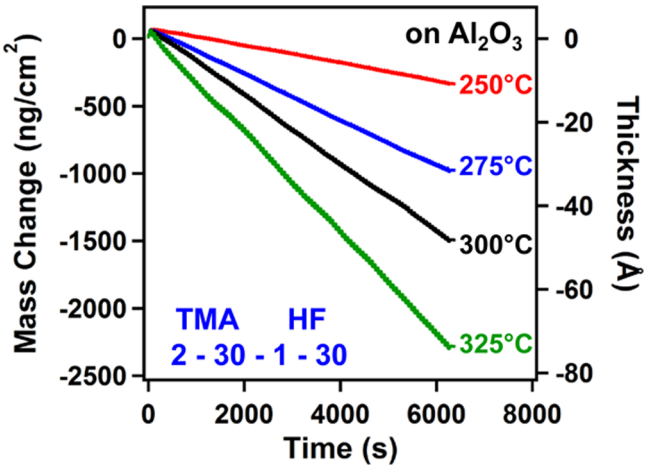

Figure 5. Mass change versus time for Al_2O_3 ALE using sequential TMA and HF exposures at 250, 275, 300, and 325 °C.

30−1−30. The initial Al_2O_3 ALD films were grown by 100 cycles of Al_2O_3 ALD at the same temperatures. The mass changes versus time during Al_2O_3 ALE are linear at all temperatures. The MCPC increases with temperature from −4.2 ng/(cm^2 cycle) at 250 °C to −23.3 ng/(cm^2 cycle) at 325 °C. These MCPCs correspond to etch rates that increase from 0.14 Å/cycle at 250 °C to 0.75 Å/cycle at 325 °C. The determination of these etch rates is based on the Al_2O_3 ALD film density of 3.1 g/cm^3. These results indicate that the Al_2O_3 etch rate can be controlled by the reaction temperature.

The nucleation of Al_2O_3 ALE was examined at different temperatures during the first several TMA and HF exposures. Figure 6 shows an enlargement of the mass changes during the first two Al_2O_3 ALE cycles for the different temperatures in Figure 5. The first TMA exposure displays mass gains of ΔM_{TMA} = 27−32 ng/cm^2 at 250−325 °C. These mass gains result from the reaction of AlOH* surface species with TMA according to $AlOH^* + Al(CH_3)_3 \rightarrow AlOAl(CH_3)_2^* + CH_4$.

The first HF exposure in Figure 6 then shows mass gains of ΔM_{HF} = 33−36 ng/cm^2 at 250−325 °C. These mass gains result from the reaction of $AlCH_3$* surface species with HF according to $AlCH_3^* + HF \rightarrow AlF^* + CH_4$. In addition, some of the underlying Al_2O_3 is also converted to an AlF_3 surface layer. The fluorination reaction $Al_2O_3 + 6HF \rightarrow 2AlF_3 + 3H_2O$ is spontaneous over the temperature range from 250 to 325 °C. The Gibbs free energy changes are negative and change slightly from ΔG= −53.8 kcal at 250 °C to ΔG = −46.8 kcal at 325 °C.[27] Figure 6 shows that the fluorination of Al_2O_3 to form an $2AlF_3$ surface layer is nearly constant at all temperatures.

DOI: 10.1021/acs.chemmater.6b00111
Chem. Mater. 2016, 28, 2994−3003

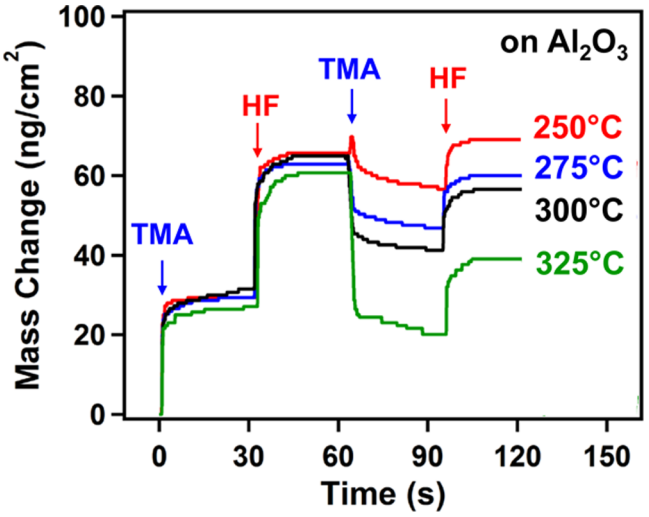

Figure 6. Expansion of first two ALE cycles in Figure 5 showing the individual mass changes during the sequential TMA and HF exposures at 250, 275, 300, and 325 °C.

HF exposures on initial, hydroxylated Al_2O_3 substrates prior to TMA exposures showed very similar mass gains of ΔM_{HF} = 35−38 ng/cm^2 at 150−250 °C.[7] This similarity of the mass gains for HF exposure on the initial hydroxylated Al_2O_3 substrate and for HF exposure on the Al_2O_3 substrate after the TMA exposure results from the similar molar mass of the $AlCH_3$* and AlOH* species. The $AlCH_3$* and AlOH* species lead to the production of CH_4 and H_2O, respectively. The mass changes resulting from these reactions, together with the mass gains occurring during the fluorination of Al_2O_3 to produce an AlF_3 surface layer, are nearly equivalent.

The mass gain of ΔM_{HF} = 33−36 ng/cm^2 at 250−325 °C can be employed to estimate the thickness of the AlF_3 surface layer on the Al_2O_3 substrate. This estimation assumes that the mass change from the reaction $AlCH_3$* + HF → AlF* + CH_4 is negligible compared with the fluorination of Al_2O_3. The fluorination reaction Al_2O_3 + 6HF → 2AlF_3 + 3H_2O will result in a mass increase of 65%. This mass increase is expected from the masses of 102 amu for Al_2O_3 and 168 amu for 2AlF_3. Therefore, the average value of ΔM_{HF} = 34 ng/cm^2 corresponds to the conversion of 52.5 ng/cm^2 of Al_2O_3 into 86.5 ng/cm^2 of the AlF_3 layer. Based on the density of 3.1 g/cm^3 for Al_2O_3,[22] the mass of 52.5 ng/cm^2 for Al_2O_3 is equivalent to an Al_2O_3 thickness of 1.7 Å. Likewise, based on the density of 2.9 g/cm^3 for AlF_3,[22] the mass of 86.5 ng/cm^2 for AlF_3 is equivalent to an AlF_3 thickness of 3.0 Å.

XPS measurements also examined the film composition after the HF exposures during Al_2O_3 ALE at 300 °C. The Al_2O_3 films were exposed to atmosphere after the Al_2O_3 ALE and prior to the XPS studies. The XPS analysis yielded F concentrations of 4−6 at. % including the adventitious carbon. Fluorine concentrations of 4−6 at. % are in approximate agreement with the expected photoelectron yield from a layered sample consisting of a 6 Å thick adventitious carbon layer[35] on a 3 Å thick AlF_3 layer on an Al_2O_3 substrate. The model for the photoelectron sources employed the C, F, Al and O number densities in each layer and the Beer−Lambert equation integrated over the film thicknesses. The Beer−Lambert equation is I = I_0 exp[-d/λ sin Θ] where I_0 is the initial photoelectron intensity, d is the distance traveled through the layer and Θ is the angle to the surface normal.[36] The electron mean free path, λ, was based on approximate expressions for λ given in the literature.[37]

After the first HF exposure, the next TMA exposure removes the AlF_3 layer on the Al_2O_3 substrate. Figure 6 shows that mass losses during the TMA and HF cycles begin with the second TMA and HF cycle for temperatures from 275−325 °C. The TMA and HF cycles at 250 °C show a mass loss after the third ALE cycle. Figure 6 reveals that higher temperatures produce both a larger mass loss for the removal of AlF_3 by TMA and a larger mass gain for the subsequent fluorination of Al_2O_3 by HF.

Figure 7 shows enlargements of the mass changes during three cycles in the steady state etching regime for Al_2O_3 ALE at

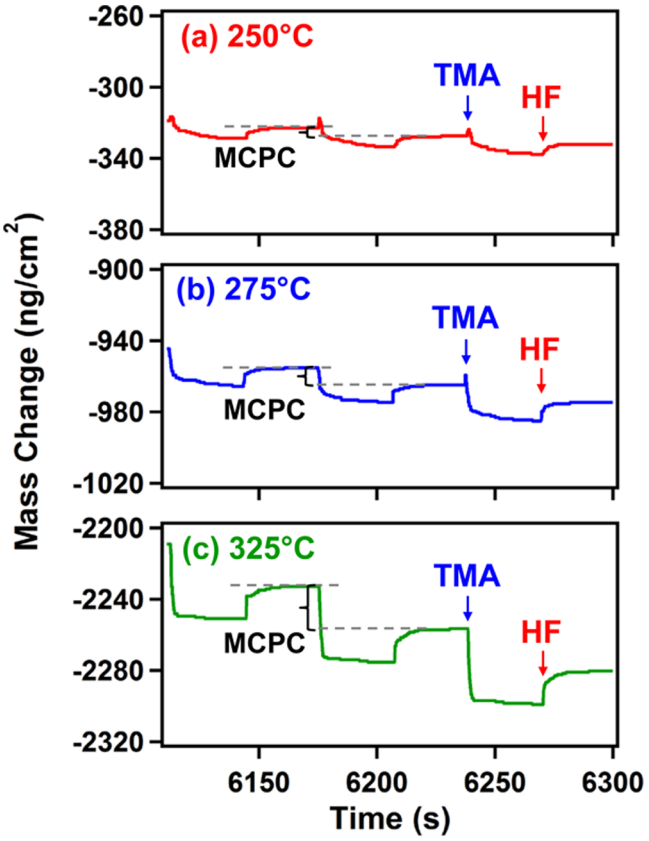

Figure 7. Enlargement of linear region of Figure 5 showing the individual mass changes during the sequential TMA and HF exposures at (a) 250, (b) 275 and (c) 325 °C.

250, 275, and 325 °C. Mass losses are observed after the TMA exposures. These mass losses suggest that $Al(CH_3)_3$ can remove the AlF_3 surface layer as volatile $AlF(CH_3)_2$ product according to the reactions AlF_3* + $Al(CH_3)_3$ → AlF_2CH_3* + $AlF(CH_3)_2$ and $AlF_2(CH_3)$* + $Al(CH_3)_3$ → 2$AlF(CH_3)_2$. Earlier experiments observed the continuous etching of an AlF_3 film by $Al(CH_3)_3$ at 300 °C.[10] This behavior suggests that the formation of volatile $AlF(CH_3)_2$ product is favorable. Mass spectrometry studies are needed to confirm these proposed volatile reaction products.

The mass losses are larger at higher temperatures. A small mass decrease is observed after the TMA exposure at 250 °C. Figure 7a displays a mass loss of ΔM_{TMA} = −10.5 ng/cm^2 after the TMA exposure for 2.0 s at 250 °C. Larger mass decreases are observed after the TMA exposures at 275 and 325 °C. Figures 7b shows a mass loss of ΔM_{TMA} = −20.5 ng/cm^2 after a

DOI: 10.1021/acs.chemmater.6b00111
Chem. Mater. 2016, 28, 2994−3003

Table 1. MCPC, Etch Rate, ΔM_{TMA}, ΔM_{HF}, Ratio, x, xMCPC, and %AlF_3 removed for Al_2O_3 ALE at Different Temperatures

temperature (°C)	MCPC ng/(cm^2 cycle)	etch rate (Å/cycle)	ΔM_{TMA} ng/(cm^2 cycle)	ΔM_{HF} ng/(cm^2 cycle)	ratio	x	xMCPC	%AlF_3 removed
250	−4.2	0.14	−10.5	6.3	2.55	7.7	−32	19
275	−10.6	0.34	−20.5	9.9	1.94	2.5	−27	38
300	−15.9	0.51	−29.0	13.1	1.83	1.6	−25	55
325	−23.3	0.75	−41.9	18.6	1.81	1.4	−33	74

TMA exposure for 2.0 s at 275 °C. Figure 7c displays an even larger mass loss of ΔM_{TMA} = −41.9 ng/cm^2 after a TMA exposure for 2.0 s at 325 °C.

In contrast, mass increases are observed after the HF fluorination reactions. These mass increases are consistent with the fluorination of Al_2O_3 to AlF_3. A mass increase of ΔM_{HF} = 6.3 ng/cm^2 is observed after the HF exposure for 1.0 s at 250 °C as shown in Figure 7a. HF exposures for 1.0 s produce larger mass gains of ΔM_{HF} = 9.9 ng/cm^2 at 275 °C and ΔM_{HF} = 18.6 ng/cm^2 at 325 °C as shown in Figures 7b and 7c, respectively. However, these ΔM_{HF} values in the steady state regime are much less than the ΔM_{HF} values observed in the first Al_2O_3 ALE cycle on initial, hydroxylated Al_2O_3 substrates in Figure 6. The smaller mass gains observed for ΔM_{HF} in the steady state regime suggest that the HF exposures may be removing surface species in addition to fluorinating Al_2O_3. The TMA exposures may also not be removing all the AlF_3 layer prior to the subsequent HF fluorination reaction.

From the QCM measurements in Figure 6, the average value of ΔM_{HF} = 34 ng/cm^2 during the first HF exposure corresponds to the conversion of 52.5 ng/cm^2 of Al_2O_3 into 86.5 ng/cm^2 of the AlF_3 layer. If TMA can remove the entire AlF_3 layer on Al_2O_3, then ΔM_{TMA} is limited to a maximum value of ΔM_{TMA} = −86.5 ng/cm^2. Because TMA can also form $AlCH_3$* surface species after AlF_3 removal, the $AlCH_3$* surface species could add 30 ng/cm^2 based on the averaged results for the first TMA exposure on the Al_2O_3 substrate at different temperatures shown in Figure 6. Consequently, ΔM_{TMA} is limited to a maximum value of ΔM_{TMA} = −56.5 ng/cm^2.

Calculations were performed to estimate the amount of AlF_3 removal during the TMA exposures at different temperatures using the measured ΔM_{TMA} values. The percentage of AlF_3 removed is based on the maximum value of ΔM_{TMA} = −56.5 ng/cm^2 expected if the entire AlF_3 layer is removed by TMA. These calculations revealed that the percentage of AlF_3 removed by the TMA exposures increases with temperature. The percentages increased from 19% at 250 °C to 74% at 325 °C. The percentages of AlF_3 removal at all the temperatures are summarized in Table 1.

The ΔM_{TMA}, ΔM_{HF}, and MCPC values at all the reaction temperatures are shown in Figure 8. All ALE reactions were performed using a reaction sequence of 2−30−1−30 on initial Al_2O_3 substrates. Figure 8a displays the ΔM_{TMA} and ΔM_{HF} values obtained at different reaction temperatures. ΔM_{TMA} shows progressively larger mass losses at higher temperatures. In contrast, ΔM_{HF} reveals progressively larger mass gains at higher temperatures. The temperature dependence of ΔM_{TMA} dominates the temperature dependence observed in the MCPC shown in Figure 8b. ΔM_{TMA}, ΔM_{HF}, MCPC, the etch rate, and the ΔM_{TMA}/MCPC ratio are summarized in Table 1.

III.B. XRR and SE Measurements. Al_2O_3 ALE was also examined using *ex situ* XRR studies. For these experiments, Al_2O_3 ALD films with a thickness of 141 Å were grown on Si(100) wafers at 300 °C. In addition, Al_2O_3 ALD films with a thickness of 170 Å were grown on Si(100) wafers at 200 °C.

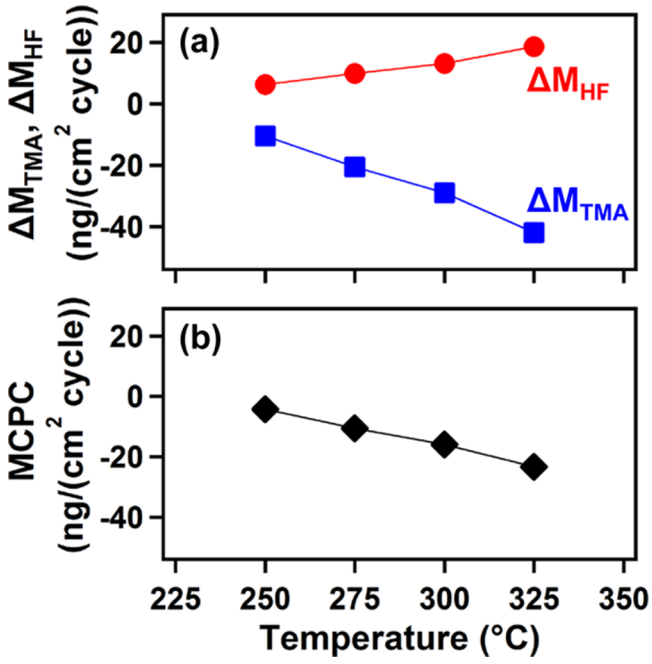

Figure 8. Temperature dependence of (a) ΔM_{TMA} and ΔM_{HF} and (b) MCPC for Al_2O_3 ALE.

These Al_2O_3 ALD films were deposited using 150 cycles of TMA and H_2O with a reaction sequence of 1−20−1−20. The XRR scans of the Al_2O_3 ALD films on the Si wafers grown at 300 °C versus the number of TMA and HF reaction cycles at 300 °C are displayed in Figure S1 in the Supporting Information.

Figure 9 shows the XRR measurements of the initial Al_2O_3 film thickness and the Al_2O_3 film thickness after 25, 50, 100, and 200 ALE cycles at 300 °C. The initial Al_2O_3 films grown at 300 and 200 °C had initial thicknesses of 141 and 170 Å, respectively. The film thickness versus number of ALE cycles in Figure 9a is linear and yields an etch rate of 0.46 Å/cycle. The spectroscopic ellipsometry (SE) measurements on these same samples also yield an etch rate of 0.46 Å/cycle. The different growth temperatures for the two Al_2O_3 films did not affect the Al_2O_3 etch rate. In addition, the etch rates determined by XRR and SE are similar to the etch rate obtained by the *in situ* QCM experiments at 300 °C.

The y intercepts from the linear least-squares fitting in Figure 9a are 142 Å for the Al_2O_3 films grown at 300 °C for both the XRR and SE measurements. These thicknesses are slightly higher than the initial thicknesses of 141 and 139 Å measured by XRR and SE, respectively. These slightly larger thicknesses originate from the mass gain that occurs during the nucleation of the ALE process on the first ALE cycle. The SE analysis also determined a refractive index of n = 1.67 for the Al_2O_3 film grown at 300 °C at a wavelength of 589 nm. This refractive index for the Al_2O_3 film remained at n = 1.68 after 25, 50, 100, and 200 ALE cycles. Similar behavior was observed for the

DOI: 10.1021/acs.chemmater.6b00111
Chem. Mater. 2016, 28, 2994−3003

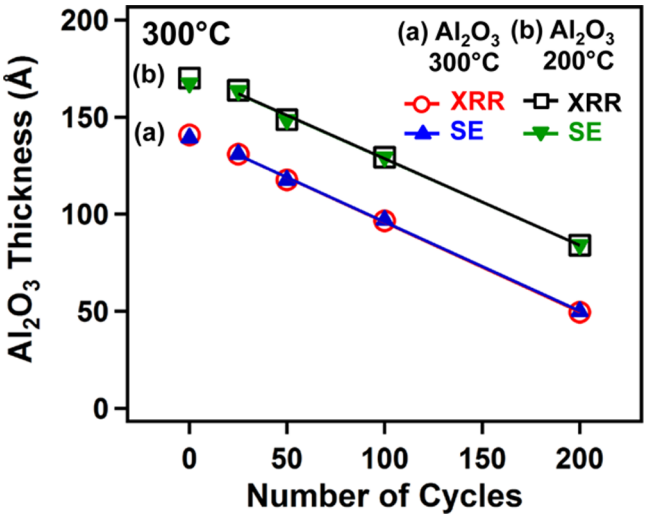

Figure 9. X-ray reflectivity and spectroscopic ellipsometry measurements of Al_2O_3 film thickness versus number of Al_2O_3 ALE cycles for initial Al_2O_3 ALD films grown using 150 Al_2O_3 ALD cycles.

Al_2O_3 films grown at 200 °C and etched at 300 °C as shown in Figure 9b.

III.C. FTIR Spectroscopy Measurements. An Al_2O_3 ALD film was first grown using 15 cycles of TMA and H_2O at 150 °C on ZrO_2 nanoparticles. FTIR spectroscopy measurements of the Al_2O_3 ALD film growth are presented in Figure S2 in the Supporting Information. Following the Al_2O_3 ALD, the sample temperature was raised to 300 °C, and the Al_2O_3 film was etched using sequential exposures of TMA and HF. FTIR spectra recorded during the TMA and HF exposures at 300 °C are shown in Figure 10. These spectra were recorded after the HF exposures and are again referenced to the starting ZrO_2 nanoparticle substrate. The progressive loss in absorbance between 800 and 1000 cm^{-1} with ALE cycles is in agreement with the etching of the Al_2O_3 film.

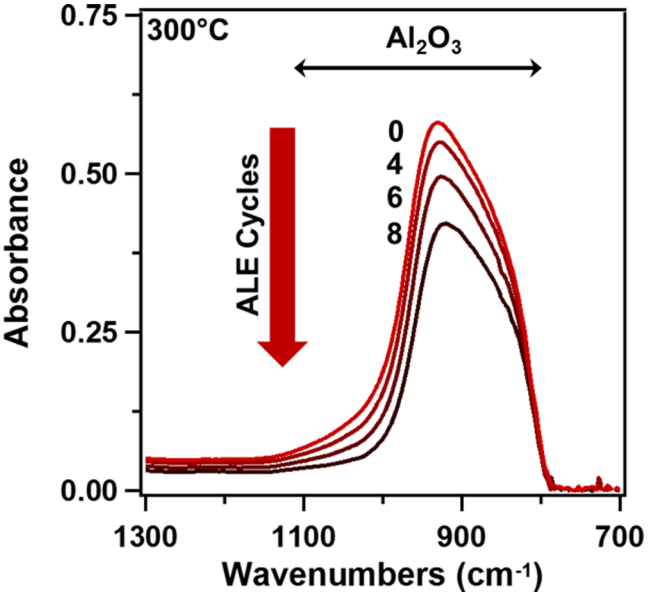

Figure 10. Infrared absorbance showing the loss of Al−O stretching vibration in bulk Al_2O_3 versus number of Al_2O_3 ALE cycles at 300 °C. These FTIR spectra were referenced to the initial ZrO_2 nanoparticles.

Figure 11 displays the FTIR difference spectra at 800−1300 cm^{-1} after consecutive TMA and HF exposures during the fifth

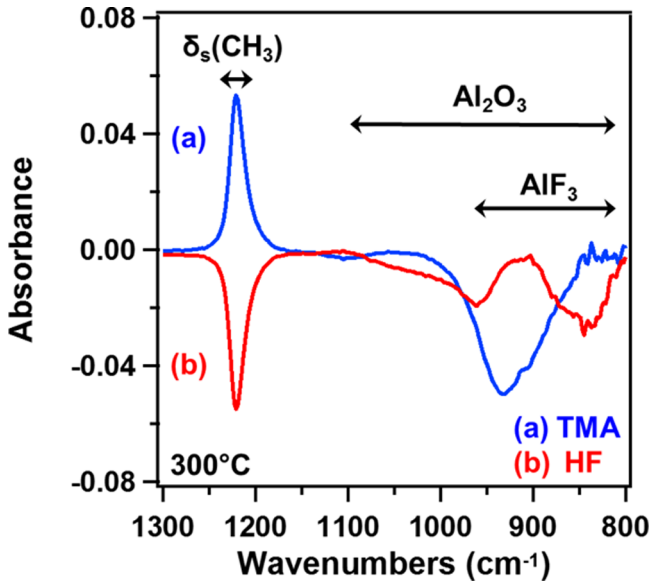

Figure 11. Difference infrared absorbance spectra from 800 to 1300 cm^{-1} during Al_2O_3 ALE at 300 °C. The difference spectra recorded after the (a) TMA and (b) HF exposures were referenced using the spectra after the previous HF and TMA exposures, respectively.

ALE cycle at 300 °C. These difference spectra are referenced to the spectra after the previous reactant exposure. After TMA exposures, an increase in absorbance at ~1212 cm^{-1} is observed in Figure 11a that is in accord with the addition of $AlCH_3$* surface species. These $AlCH_3$* species may be present as either $AlF(CH_3)_2$*, $AlF_2(CH_3)$*, or $-OAl(CH_3)_2$*. All of these species would be expected to show a methyl deformation mode at ~1212 cm^{-1}. However, since $AlF(CH_3)_2$ is expected to have a higher volatility than other species, the vibrational feature at 1212 cm^{-1} is likely attributed to $AlF_2(CH_3)$* or $-OAl(CH_3)_2$*. In addition, a decrease in absorbance between ~850 and 975 cm^{-1} is observed that is consistent with the loss of absorbance from Al−F stretching vibrations as TMA removes the AlF_3 surface layer.

Figure 11b shows the absorbance after the subsequent HF exposure. The absorbance is completely removed for the vibrational feature attributed to the addition of $AlCH_3$* species. This loss of absorbance is in accord with the conversion of $AlCH_3$* surface species to AlF* species. The HF exposure also results in a broad absorbance loss between 800 and 1100 cm^{-1} that is in agreement with the conversion of Al_2O_3 into AlF_3 by the reaction $Al_2O_3 + 6HF \rightarrow 2AlF_3 + 3H_2O$. Figure 11b also reveals an absorbance increase on the broad absorbance loss between ~850 and 950 cm^{-1} that is consistent with the formation of the AlF_3 layer.

Figure 12 shows the difference spectra from 2500 to 4000 cm^{-1} for the same consecutive TMA and HF exposures at 300 °C that are displayed in Figure 11. Figure 12a shows the difference spectrum after the TMA exposure. An increase in absorbance is observed at ~2900 and 2950 cm^{-1} that is in agreement with the addition of symmetric and asymmetric stretching vibrations of $AlCH_3$* species, respectively. This absorbance gain is in accord with the formation of $AlF_2(CH_3)$* or $-OAl(CH_3)_2$* species after TMA exposures. Figure 12b shows the difference spectrum after the HF exposure. The

DOI: 10.1021/acs.chemmater.6b00111
Chem. Mater. 2016, 28, 2994−3003

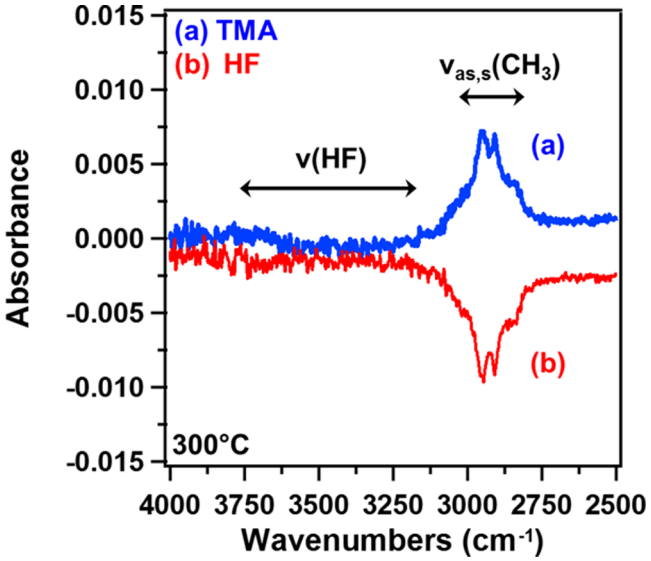

Figure 12. Difference infrared absorbance spectra from 2500 to 4000 cm^{-1} during Al_2O_3 ALE at 300 °C. The difference spectra recorded after the (a) TMA and (b) HF exposures were referenced using the spectra after the previous HF and TMA exposures, respectively.

spectrum observes an absorbance decrease at ~2900 and ~2950 cm^{-1} that is consistent with the removal of the previously added $AlCH_3$* species.

There are also no vibrational features in Figure 12a and b between ~3000 and 3675 cm^{-1} that would indicate HF* surface species. Vibrational features for HF* were observed during AlF_3 ALD using TMA and HF at lower temperatures.[22] HF* species are important intermediates during AlF_3 ALD growth. The desorption of HF* surface species at higher temperatures allows TMA to accept fluorine from the underlying AlF_3 film and form volatile etch products that lead to Al_2O_3 etching. At lower temperatures, HF* surface species remain on the surface and react with TMA to form AlF_3.[22] Temperature can determine whether TMA and HF lead to either AlF_3 ALD or Al_2O_3 ALE.

III.D. Proposed Al_2O_3 ALE Mechanism. Figure 13 shows the schematic for the proposed ALE reaction mechanism. This mechanism is based on the mass changes during the TMA and HF exposures as determined by the QCM measurements. This visualization does not include surface species that do not change during the HF and TMA reactions. During the fluorination reaction (A), HF reacts with $AlCH_3$* surface species to form AlF* surface species and CH_4 reaction product. HF also reacts with the underlying Al_2O_3 film to form an AlF_3 surface layer and H_2O as a reaction product. The AlF_3 layer is then ready for the next TMA reaction.

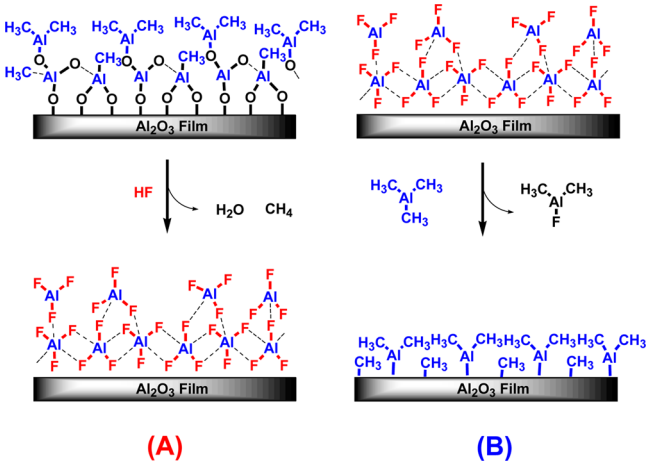

Figure 13. Schematic of proposed reaction mechanism for Al_2O_3 ALE showing (A) HF reaction and (B) TMA reaction.

During the ligand-exchange reaction (B), TMA reacts with the AlF_3 surface layer on the Al_2O_3 substrate to form volatile $AlF(CH_3)_2$ reaction products. $AlF(CH_3)_2$ has a vapor pressure of 80 Torr at 100 °C.[38] There also may be $AlF_2(CH_3)$* surface species produced by the TMA exposures. These $AlF_2(CH_3)$* surface species could be removed by additional TMA exposure. The reaction for the removal of $AlF_2(CH_3)$* surface species is $Al(CH_3)_3 + AlF_2(CH_3)^* \rightarrow 2AlF(CH_3)_2$. After the removal of fluorine-containing species, $Al(CH_3)_3$ could also react with the underlying Al_2O_3 substrate to form $Al(CH_3)$*.

The simplest overall proposed reaction can be expressed as

$$Al_2O_3 + 6HF + 4Al(CH_3)_3 \rightarrow 6AlF(CH_3)_2 + 3H_2O \quad (1)$$

This overall reaction can be divided into the HF and TMA reactions:

$$(A)Al_2O_3|Al_2O_3\dagger + 6HF \rightarrow Al_2O_3|2AlF_3\dagger + 3H_2O \quad (2)$$

$$(B)Al_2O_3|2AlF_3\dagger + 4Al(CH_3)_3 \rightarrow Al_2O_3\dagger + 6AlF(CH_3)_2 \quad (3)$$

The daggers indicate the species involved in the etching, and the vertical lines are used to separate the various surface species. The amount of Al_2O_3 that is etched during the ALE reactions is given by $Al_2O_3\dagger$ in eqs 2 and 3.

The reactions described by eqs 1−3 are incomplete because TMA can also interact with the etched surface. For example, the reaction of TMA with Al_2O_3 is known to form $AlCH_3$* surface species.[39] This reaction of $Al(CH_3)_3$ with Al−O−Al bonds on the Al_2O_3 substrate can be expressed as

$$Al{-}O{-}Al^* + Al(CH_3)_3 \rightarrow Al{-}O{-}Al(CH_3)_2{}^* + Al(CH_3)^* \quad (4)$$

TMA may also interact with AlF_3 species remaining on the etched surface. To incorporate the $Al(CH_3)_3$* species, the HF and TMA reactions need be modified:

$$(A)\ Al_2O_3|xAl(CH_3)_3{}^* + (6+3x)HF \rightarrow 2AlF_3|xAlF_3{}^* + 3H_2O + 3xCH_4 \quad (5)$$

$$(B)\ 2AlF_3|xAlF_3{}^* + (4+3x)Al(CH_3)_3 \rightarrow xAl(CH_3)_3{}^* + (6+3x)AlF(CH_3)_2 \quad (6)$$

The conventions are slightly different in the HF and TMA reactions given by eqs 2 and 3 and eqs 5 and 6. The amount of Al_2O_3 that is etched during the ALE reactions is given by Al_2O_3 in eqs 5 and 6. x is a parameter that defines the number of $Al(CH_3)_3$* species relative to the number of Al_2O_3 units that are etched during the ALE reaction.

The overall proposed reaction can then be expressed as

$$Al_2O_3 + (6+3x)HF + (4+3x)Al(CH_3)_3 \rightarrow (6+3x)AlF(CH_3)_2 + 3H_2O + 3xCH_4 \quad (7)$$

DOI: 10.1021/acs.chemmater.6b00111
Chem. Mater. 2016, 28, 2994−3003

x can be calculated from the ΔM_{TMA}/MCPC ratio using the equation:

$$x = (2 \times 84 - 102(\Delta M_{TMA}/\mathrm{MCPC}))/(72 - 84) \quad (8)$$

where 84, 102, and 72 are the molecular weights for AlF_3, Al_2O_3, and $Al(CH_3)_3$, respectively. To obtain agreement with the relative ΔM_{TMA} and ΔM_{HF} mass changes in Table 1, x = 7.7, 2.5, 1.6, and 1.4 at 250, 275, 300, and 325 °C, respectively.

Although x decreases at higher temperatures, the product xMCPC is fairly constant over the entire temperature range. This behavior results from the increase in MCPC and the decrease in x at higher temperatures. These temperature dependences yield a nearly constant xMCPC product versus temperature. Because x is defined relative to the amount of Al_2O_3 that is etched during the ALE reaction, the absolute $Al(CH_3)_3$* coverages are proportional to xMCPC. The nearly constant xMCPC values in Table 1 indicate that the absolute $Al(CH_3)_3$* coverages are similar at all the etching temperatures. The larger etch rates at higher temperatures are attributed to the higher percentage of the AlF_3 surface layer removed by ligand-exchange reactions during TMA exposures at higher temperatures.

IV. CONCLUSIONS

Al_2O_3 ALE was demonstrated using sequential, self-limiting thermal reactions with HF and TMA as the reactants. TMA is an effective metal precursor for the ligand-exchange transmetalation reaction during thermal ALE. Al_2O_3 ALD can be performed using TMA and H_2O. Al_2O_3 ALE can be accomplished using TMA and HF. The ability of TMA to lead to either Al_2O_3 ALD or Al_2O_3 ALE suggests that metal ALD precursors for a particular material may also be employed for the ALE of the same material.

Al_2O_3 ALE was studied at temperatures from 250 to 325 °C using QCM experiments. The QCM studies revealed that the Al_2O_3 ALE was linear versus the number of HF and TMA reaction cycles. The sequential HF and TMA reactions were self-limiting versus reactant exposure. The Al_2O_3 etching rates were larger at higher temperatures. The etch rates varied from 0.14 Å/cycle at 250 °C to 0.75 Å/cycle at 325 °C. XRR and SE studies confirmed the linearity of Al_2O_3 ALE and the etching rates. FTIR spectroscopy studies observed the loss of infrared absorbance from the Al−O stretching vibrations during Al_2O_3 ALE. The FTIR studies also identified AlF* surface species after the HF exposures and $AlCH_3$* species after the TMA exposures.

The overall reaction for Al_2O_3 ALE is believed to be described by $Al_2O_3 + 4Al(CH_3)_3 + 6HF \rightarrow 6AlF(CH_3)_2 + 3H_2O$. This overall reaction is the result of individual fluorination and ligand-exchange reactions. The HF exposure fluorinates the Al_2O_3 substrate and forms an AlF_3 surface layer and H_2O as the reaction products. In a ligand-exchange transmetalation reaction, TMA accepts F from the AlF_3 layer and donates CH_3 to the AlF_3 layer to produce volatile $AlF(CH_3)_2$ reaction products. The AlF_3 surface layer was estimated to have a thickness of 3.0 Å on Al_2O_3 after the HF exposures. The larger etch rates at higher temperatures result from the removal of a larger fraction of the AlF_3 surface layer by TMA at higher temperatures. The ability to change the metal precursor and the ligands during the ligand-exchange reaction may also provide pathways to selective ALE.

■ ASSOCIATED CONTENT

Supporting Information

The Supporting Information is available free of charge on the ACS Publications website at DOI: 10.1021/acs.chemmater.6b00111.

XRR measurements of Al_2O_3 ALE versus number of TMA and HF reaction cycles at 300 °C; FTIR spectroscopy measurements of Al_2O_3 ALD versus number of TMA and H_2O reaction cycles at 150 °C (PDF)

■ AUTHOR INFORMATION

Corresponding Author

*E-mail: steven.george@colorado.edu.

Notes

The authors declare no competing financial interest.

■ ACKNOWLEDGMENTS

This research was funded by the National Science Foundation (CHE-1306131). Additional support was provided by Intel Corporation through a Member Specific Research Project administered by the Semiconductor Research Corporation. The authors acknowledge Dr. Huaxing Sun for obtaining and modeling the XPS results.

■ REFERENCES

(1) Kanarik, K. J.; Lill, T.; Hudson, E. A.; Sriraman, S.; Tan, S.; Marks, J.; Vahedi, V.; Gottscho, R. A. Overview of Atomic Layer Etching in the Semiconductor Industry. *J. Vac. Sci. Technol., A* **2015**, *33*, 020802.

(2) Carver, C. T.; Plombon, J. J.; Romero, P. E.; Suri, S.; Tronic, T. A.; Turkot, R. B. Atomic Layer Etching: An Industry Perspective. *ECS J. Solid State Sci. Technol.* **2015**, *4*, N5005−N5009.

(3) George, S. M. Atomic Layer Deposition: An Overview. *Chem. Rev.* **2010**, *110*, 111−131.

(4) Faraz, T.; Roozeboom, F.; Knoops, H. C. M.; Kessels, W. M. M. Atomic Layer Etching: What Can We Learn from Atomic Layer Deposition? *ECS J. Solid State Sci. Technol.* **2015**, *4*, N5023−N5032.

(5) Agarwal, A.; Kushner, M. J. Plasma Atomic Layer Etching Using Conventional Plasma Equipment. *J. Vac. Sci. Technol., A* **2009**, *27*, 37−50.

(6) Oehrlein, G. S.; Metzler, D.; Li, C. Atomic Layer Etching at the Tipping Point: An Overview. *ECS J. Solid State Sci. Technol.* **2015**, *4*, N5041−N5053.

(7) Lee, Y.; DuMont, J. W.; George, S. M. Mechanism of Thermal Al_2O_3 Atomic Layer Etching Using Sequential Reactions with $Sn(acac)_2$ and HF. *Chem. Mater.* **2015**, *27*, 3648−3657.

(8) Lee, Y.; George, S. M. Atomic Layer Etching of Al_2O_3 Using Sequential, Self-Limiting Thermal Reactions with $Sn(acac)_2$ and HF. *ACS Nano* **2015**, *9*, 2061−2070.

(9) Lee, Y.; DuMont, J. W.; George, S. M. Atomic Layer Etching of HfO_2 Using Sequential, Self-Limiting Thermal Reactions with $Sn(acac)_2$ and HF. *ECS J. Solid State Sci. Technol.* **2015**, *4*, N5013−N5022.

(10) Lee, Y.; DuMont, J. W.; George, S. M. Atomic Layer Etching of AlF_3 Using Sequential, Self-Limiting Thermal Reactions with $Sn(acac)_2$ and Hydrogen Fluoride. *J. Phys. Chem. C* **2015**, *119*, 25385−25393.

(11) Osakada, K. Transmetalation. In *Fundamentals of Molecular Catalysis, Current Methods in Inorganic Chemistry*; Kurosawa, H., Yamamoto, A., Eds.; Elsevier Science: Amsterdam, 2003; Vol. 3.

(12) Lockhart, J. C. Redistribution and Exchange Reactions in Groups IIB-VIIB. *Chem. Rev.* **1965**, *65*, 131−151.

(13) Spessard, G. O.; Miessler, G. L. *Organometallic Chemistry*, 3rd. ed.; Oxford University Press: New York, 2016.

DOI: 10.1021/acs.chemmater.6b00111
Chem. Mater. 2016, 28, 2994−3003

(14) Roesky, H. W.; Haiduc, I. Fluorine as a Structure-Directing Element in Organometallic Fluorides: Discrete Molecules, Supramolecular Self-Assembly and Host-Guest Complexation. *J. Chem. Soc., Dalton Trans.* **1999**, 2249−2264.
(15) Janiak, C. Stannocene as Cyclopentadienyl Transfer Agent in Transmetalation Reactions with Lanthanide Metals for the Synthesis of Tris(cyclopentadienyl)lanthanides. *Z. Anorg. Allg. Chem.* **2010**, *636*, 2387−2390.
(16) Westerhausen, M. Synthesis and Spectroscopic Properties of Bis(trimethylsilyl)amides of the Alkaline-Earth Metals Magnesium, Calcium, Strontium, and Barium. *Inorg. Chem.* **1991**, *30*, 96−101.
(17) Davies, A. G.; Gielen, M.; Pannell, K. H.; Tiekink, E. R. T. *Tin Chemistry: Fundamentals, Frontiers and Applications*; John Wiley & Sons, Ltd.: West Sussex, United Kingdom, 2008.
(18) Ewings, P. F. R.; Harrison, P. G.; Fenton, D. E. Derivatives of Divalent Germanium, Tin, and Lead. 5. Bis-(Pentane-2,4-Dionato)-Tin(II),Bis(1,1,1-Trifluoropentane-2,4-Dionato)-Tin(II), and Bis-(1,1,1,5,5,5-Hexafluoropentane-2,4-Dionato)-Tin(II). *J. Chem. Soc., Dalton Trans.* **1975**, 821−826.
(19) Darwent, B. d. B. *Bond Dissociation Energies in Simple Molecules*; National Bureau of Standards, United States Department of Commerce: Washington, DC, 1970.
(20) Puurunen, R. L. Surface Chemistry of Atomic Layer Deposition: A Case Study for the Trimethylaluminum/Water Process. *J. Appl. Phys.* **2005**, *97*, 121301.
(21) Elam, J. W.; Groner, M. D.; George, S. M. Viscous Flow Reactor with Quartz Crystal Microbalance for Thin Film Growth by Atomic Layer Deposition. *Rev. Sci. Instrum.* **2002**, *73*, 2981−2987.
(22) Lee, Y.; DuMont, J. W.; Cavanagh, A. S.; George, S. M. Atomic Layer Deposition of AlF_3 Using Trimethylaluminum and Hydrogen Fluoride. *J. Phys. Chem. C* **2015**, *119*, 14185−14194.
(23) Shannon, R. D.; Shannon, R. C.; Medenbach, O.; Fischer, R. X. Refractive Index and Dispersion of Fluorides and Oxides. *J. Phys. Chem. Ref. Data* **2002**, *31*, 931−970.
(24) DuMont, J. W.; George, S. M. Pyrolysis of Alucone Molecular Layer Deposition Films Studied Using In Situ Transmission Fourier Transform Infrared Spectroscopy. *J. Phys. Chem. C* **2015**, *119*, 14603−14612.
(25) Ballinger, T. H.; Wong, J. C. S.; Yates, J. T. Transmission Infrared-Spectroscopy of High Area Solid-Surfaces - A Useful Method for Sample Preparation. *Langmuir* **1992**, *8*, 1676−1678.
(26) Ferguson, J. D.; Weimer, A. W.; George, S. M. Atomic Layer Deposition of Ultrathin and Conformal Al_2O_3 films on BN Particles. *Thin Solid Films* **2000**, *371*, 95−104.
(27) *HSC Chemistry 5.1*; Outokumpu Research Oy: Pori, Finland.
(28) Evertsson, J.; Bertram, F.; Zhang, F.; Rullik, L.; Merte, L. R.; Shipilin, M.; Soldemo, M.; Ahmadi, S.; Vinogradov, N.; Carlà, F.; Weissenrieder, J.; Göthelid, M.; Pan, J.; Mikkelsen, A.; Nilsson, J. O.; Lundgren, E. The Thickness of Native Oxides on Aluminum Alloys and Single Crystals. *Appl. Surf. Sci.* **2015**, *349*, 826−832.
(29) Graham, M. J.; Cohen, M. On the Mechanism of Low Temperature Oxidation (23−450 C) of Polycrystalline Nickel. *J. Electrochem. Soc.* **1972**, *119*, 879−882.
(30) Song, S.; Placido, F. Investigation on Initial Oxidation Kinetics of Al, Ni, and Hf Metal Film Surfaces. *Chin. Opt. Lett.* **2010**, *8*, 87−90.
(31) Derrie, J.; Commandre, M. SiO_2 Ultra Thin Film Growth Kinetics as Investigated by Surface Techniques. *Surf. Sci.* **1982**, *118*, 32−46.
(32) Fehlner, F. P. Formation of Ultrathin Oxide Films on Silicon. *J. Electrochem. Soc.* **1972**, *119*, 1723−1727.
(33) Gupta, P.; Mak, C. H.; Coon, P. A.; George, S. M. Oxidation Kinetics of Si(111)7 × 7 in the Submonolayer Regime. *Phys. Rev. B: Condens. Matter Mater. Phys.* **1989**, *40*, 7739−7749.
(34) Pilling, N. B.; Bedworth, R. E. The Oxidation of Metals at High Temperatures. *J. Inst. Met.* **1923**, *29*, 529−582.
(35) Mangolini, F.; McClimon, J. B.; Rose, F.; Carpick, R. W. Accounting for Nanometer-Thick Adventitious Carbon Contamination in X-ray Absorption Spectra of Carbon-Based Materials. *Anal. Chem.* **2014**, *86*, 12258−12265.
(36) Castle, J. E. Use of X-Ray Photoelectron Spectroscopy in Corrosion Science. *Surf. Sci.* **1977**, *68*, 583−602.
(37) Seah, M. P.; Dench, W. A. Quantitative Electron Spectroscopy of Surfaces: A Standard Data Base for Electron Inelastic Mean Free Paths in Solids. *Surf. Interface Anal.* **1979**, *1*, 2−11.
(38) Weidlein, J.; Krieg, V. Vibrational Spectra of Dimethyl and Diethyl Aluminum Fluoride. *J. Organomet. Chem.* **1968**, *11*, 9−16.
(39) Dillon, A. C.; Ott, A. W.; Way, J. D.; George, S. M. Surface Chemistry of Al_2O_3 Deposition Using $Al(CH_3)_3$ and H_2O in a Binary Reaction Sequence. *Surf. Sci.* **1995**, *322*, 230−242.

DOI: 10.1021/acs.chemmater.6b00111
Chem. Mater. 2016, 28, 2994−3003